Real-Time Information Systems for Seismic Hazards Mitigation UrEDAS, HERAS and PIC

Yutaka NAKAMURA
General manager, UrEDAS R&D Promotion Department

Constructing strong structures and facilities is an essential countermeasure in Earthquake Disaster Prevention (EDP). For railway systems, the safety of passengers from strong motion is a big concern regarding safety and stability of running trains. The EDP, in general, requires not only the hardware measures but also the software measures to minimize the influence of earthquake damage. In this paper, basic concepts of the EDP are described and the real-time earthquake information systems, UrEDAS, Urgent Earthquake Detection and Alarm System, and HERAS, Hazards Estimation and Restoration Aid System, are outlined. Furthermore, as the elementary techniques of these systems, investigation methods using PIC, Portable Intelligent Collector, and vulnerability indexes K values for surface of ground and structures are proposed.

Key words: Earthquake warning system, UrEDAS, quick-response system, HERAS, microtremor, PIC, spectral ratio, QTS, vulnerability index, K-values, hazard estimation

1. BASIC CONCEPT OF EARTHQUAKE DISASTER PREVENTION

Earthquake disaster countermeasures are based in principle to know both characteristics of earthquake motions and resisting power of structures against the earthquake motions. Earthquake damage occurs when earthquake power exceeds the resisting power or durability of the structures, including natural ones such as slopes. Disaster can be prevented if we have found weak points of structures beforehand and executed effective countermeasures in advance. Thus, it is really important to assume a few kinds of earthquakes which may attack the area and to clarify the weak points of structures by estimating the expected earthquake damage. However, practically it is impossible to reinforce all estimated weak points before the earthquake.

Thus, the following two points become indispensable for the earthquake disaster prevention, namely:

1) to estimate the present anti-seismic durability of existing structures, and
2) to prepare always back-up countermeasures to avoid an unexpected hazardous situation.

The second item is a co-seismic countermeasure and it asks real-time response. For the first item, it is necessary to grasp the change of durability degree in time by measuring it with appropriate intervals.

2. CONTINUOUS MONITORING OF EARTHQUAKE OCCURRENCE

2.1 Alarm Seismometer

Since the second half of the 1950s simple alarm seismometers have been installed along the railway in Japan by the Japan National Railway at that time. Along the Tokaido Shinkansen, which started its operation in October 1964, the same alarm seismometers were also installed. A local earthquake (M6.1) near Shizuoka in April 1965, signaled the urgency to prepare an automatic train stop system using more reliable alarm seismometers. However, though the newly adopted alarm seismometer issues an alarm when seismic acceleration exceeds a pre-set threshold, it can not give the final maximum acceleration experienced. When Tohoku Shinkansen was opened in 1982, the alarm seismometer was developed to set several alarm acceleration levels and indicate the maximum acceleration value with a print-out as well as to give analog waveform records. Since then similar alarm seismometers have been introduced for the conventional JR, Japan Railways, lines and other Shinkansens and now its number is more than four hundred. The alarm seismometers are at present installed every 40−50 km along the conventional lines of JR and about every 20 km along the Shinkansens.

The alarm seismometer is installed on the ground surface and an alarm is issued when horizontal acceleration exceeds about 40 Gal. The alarm is issued generally after S-wave arrives. If we set the threshold level lower, the seismic motion can be detected earlier. However, it easily responds to many environmental noise due to human activities such as traffic vibrations and industries and increases false alarms. Conventional alarm seismometers include the two following problems,

1) alarm comes too late to give enough time useful for the countermeasures, and
2) frequent false alarm is issued for the harmless small earthquakes.

The above problems are based on the basic idea to issue an alarm, when seismic motion exceeds the pre-set threshold level. Thus the problems can not be solved even when we use quantities other than the acceleration.

2.2 Earthquake Early Warning

In order to realize the early detection of an earthquake, the two following methods will be discussed,

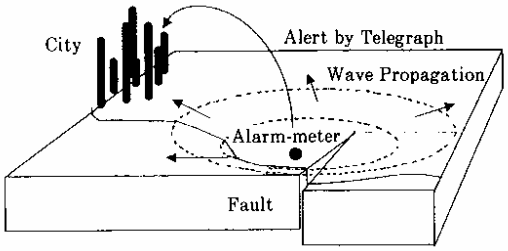

Fig. 1 Concept of the Front Alarm by Dr. J. D. Cooper.

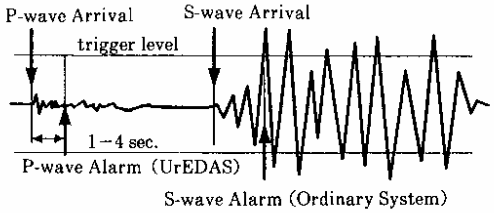

Fig. 2 Timing of the alarms.

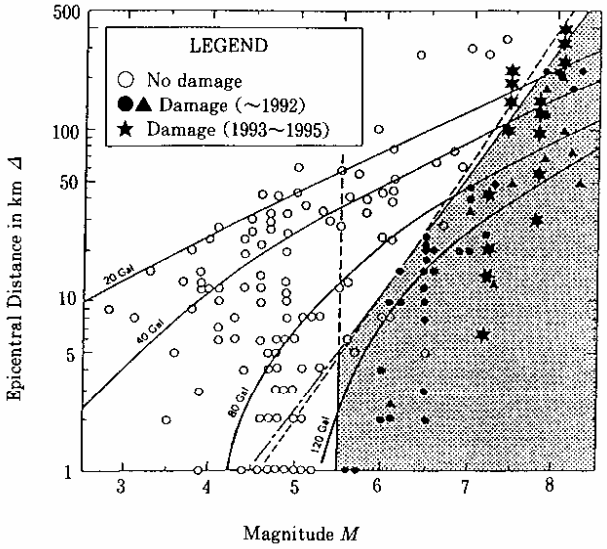

Fig. 3 Earthquake railway damage onM-Δ plane.

1)to detect the earthquake near the epicentral area, which is named as "Front alarm", and
2)to detect the earthquake by initial P-wave, which is named as "P-wave alarm".

(1) Front Alarm

The idea of front alarm is explained in Fig. 1. The earthquake motions are detected as early as possible near the source to prepare against the earthquake before seismic motion reaches the site, using the difference of transmission velocities, electric communication (=300,000 km/s) and seismic wave (≅ 8 km/s). This idea was first published in the San Francisco Daily Evening Bulletin, 3rd Nov. 1868, by J.D.Cooper, M.D. in San Francisco (Nakamura and Tucker, 1988). He described the necessity of automation of the early warning system and problem of false alarm as well as the importance of public education for the warning. However, the technical level at that time could not realize his idea in practice. After about 100 years, in 1972, Dr. Motohiko Hakuno(the then professor of Earthquake Research Institute, Univ. of Tokyo) and others proposed the same idea of Dr. J. D. Cooper for Tokyo instead of San Francisco. The then Japanese National Railways paid strong interest in this concept as a new installation to prepare against unexpected situations of railways due to strong earthquakes and promoted the research and development for this project. Thus JNR completed the Coast-line Detection System for the Tohoku Shinkansen in 1982 (Nakamura and Saito, 1982). The Mexico City Seismic Alert System, almost the same as the JNR Coast-line Detection System, was installed in 1991 (Espinosa-Aranda, et al., 1995).

(2) P-wave Alarm

Fig. 2 shows timing of the alarms in relation to the seismic motion schematically. Conventional alarm seismometers detect earthquake motion when the main motion arrives (S-wave alarm). An alarm can be issued earlier if we detect the earthquake by P-wave. However, P-wave alarm is not very easy because it issues an alarm merely when the earthquake motion exceeds a certain pre-set trigger level. If the trigger level is lowered, detection can be done earlier, but false alarm occurs very often.

In order to examine new alarm methods, past cases of earthquake railway damage are plotted in a diagram, taking earthquake magnitude in horizontal axis and epicentral distance in vertical axis as in Fig. 3. It clearly shows damage occurs M>5.5 and damaged areas are confined within a certain distance range around the epicenter. For example, earthquakes with M6, M7 and M8 give damage within epicentral distances 12 km, 60 km and 300 km respectively. If we could estimate the earthquake magnitude and epicenter location with depth rapidly, the area to be alarmed is clearly shown by M-Δ diagram in Fig. 3 and reasonable alarm can be issued immediately after the earthquake. This new alarm is referred to as M-Δ Alarm.

3. DEVELOPMENT AND PRACTICAL USE OF UrEDAS

UrEDAS, Urgent Earthquake Detection and Alarm System, is a uniquely practical system and it was the first real-time earthquake disaster prevention system in the world. The special feature of the system is the rapid alarm using information from P-wave data. It issues the alarm not simply because the seismic motion is strong, rather it issues the alarm for the area to be damaged using the magnitude and hypocenter data obtained by P-wave observation.

In 1983 a prototype system using a personal computer which realized the basic function of UrEDAS was completed and since 1984 its test observations were executed in Miyako, a Pacific coast city of the Tohoku District, and some other places. Then an UrEDAS network for the Tokyo

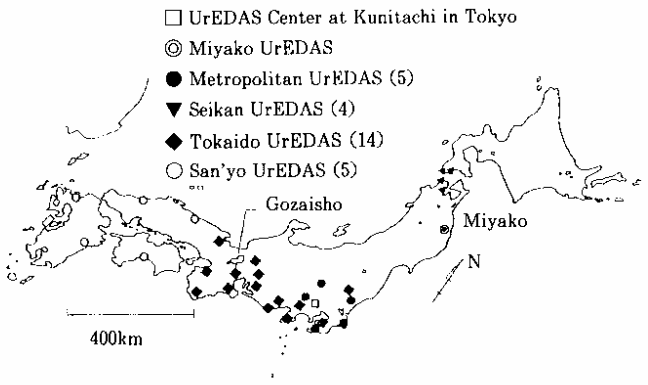

Fig. 4 Distribution of UrEDAS in Japan.

Metropolitan Area consisting of five UrEDAS was established in 1988-1989 by the subsidy of the Ministry of Transportation. In March 1988 four UrEDAS were also installed for the Seikan Under-Sea Tunnel between Honshu and Hokkaido as a part of its earthquake disaster prevention system. The Tokaido UrEDAS at Omaezaki, Shizuoka Prefecture, started limited use in September 1990, and in March 1992 fourteen UrEDAS surrounding the Tokaido Shinkansen were installed to put in practice the P-wave alarm functions (M- Δ Alarm). Since 1992, earthquake hypocenter information with map, obtained by the Metropolitan UrEDAS Network, has been delivered by facsimile to maximum 50 limited test users as real-time service about 4 minutes after each earthquake.

In September 1992, an UrEDAS was installed in Kresge Seismological Laboratory, California Institute of Technology (Caltech), Pasadena, California, USA as a joint research project of RTRI with Prof. H. Kanamori of Caltech. This Pasadena UrEDAS observed the Northridge Earthquake, 17 January 1994, and its aftershocks.

UrEDAS gives location, depth and magnitude of the earthquake in order to estimate the impending damage promptly. To know the earthquake dimension, data at many observation points are usually used. However, considering the complexity of multi-station systems and weakness of network systems, UrEDAS adopted the single station principle for the alarming.

By monitoring the earthquake motions of a single observation point in real-time, an UrEDAS detects initial P-wave motion, estimates epicenter azimuth and magnitude, calculates epicentral distance and focal depth as the first inference within about three seconds after detecting P wave. This is the actual function of UrEDAS in practical use for Tokaido Shinkansen since March 1992. With respect to the locations of epicenter and UrEDAS point, the alarm eventually reaches the target area before the P-wave arrival. UrEDAS issues the first alarm information just 1-4 sec after P-wave arrival and sends out the second information after arrival of S-wave.

Even in case of using plural UrEDAS, individual UrEDAS estimates the earthquake elements separately and sends necessary alarm by individual judgment. Information of earthquake elements decided by each individual UrEDAS is collected in the UrEDAS center and synthesized into final earthquake elements with higher accuracy. For example, the Center System of Tokaido UrEDAS automatically outputs a Re-Operation Procedure Recommendation Sheet of countermeasures for the alarmed earthquake within two minutes after P-wave arrived at the first UrEDAS station.

Ordinary centralized alarm system looses its total function when its center equipment are once destroyed. On the contrary, UrEDAS is a completely autonomous and dispersed system, and even for a destructive earthquake its system function is never out of function simultaneously. Even when main earthquake motions destroy an UrEDAS, it has already issued the alarm and necessary information has been already communicated to the necessary areas.

In addition, UrEDAS responds to big earthquakes far from the railroads, while conventional alarm seismometers function against local strong earthquakes just beneath the line and both systems compensate their roles with each other. At present, in December 1995, we have twenty five sets of UrEDAS in Japan (see Fig. 4) and one set in USA. In 1996 five sets of UrEDAS will be established for the San'yo Shinkansen and many new installations is also under planning.

3.1 Principle of UrEDAS

The warning system's task is to estimate the magnitude of an earthquake as well as its epicenter based on the seismic motion measured at a single earthquake observation point. Unlike the existing automatic seismic observation systems, this warning system does not have to transmit the observed waveform in real-time to a remote processing center and thus the system can be considerably simplified.

(1) Epicentral Azimuth

Of the seismic wave motions, the one which reaches the observation point most quickly is the P-wave, and in this case, the direction of seismic motion and the direction of wave propagation coincide. Therefore, the epicentral azimuth can be estimated from the direction of the initial motion projected on the horizontal plane. But the azimuth estimations derived simply from the amplitude ratio of EW component to NS component show large dispersions and are not accurate. The following method is therefore proposed to obtain better results (Nakamura and Saito, 1983b).

1) To estimate the cross-correlations at lag time t = 0, R_{nsud} and R_{ewud}, between vertical motion X_{ud} and horizontal motions, X_{ns} and X_{ew}, as follows,

$$R_{nsud}(i) = \alpha R_{nsud}(i-1) + X_{ns}(i)\, X_{ud}(i), \quad (1)$$

$$R_{ewud}(i) = \alpha R_{ewud}(i-1) + X_{ew}(i)\, X_{ud}(i). \quad (2)$$

2) To derive an epicentral azimuth $\Theta(i)$ from the ratio R_{nsud}/R_{ewud} for each time step i, i.e.,

$$\tan \Theta(i) = R_{nsud}(i)/R_{ewud}(i). \quad (3)$$

3) To define the average of the steady part of $\Theta(i)$ after the P-wave arrival as the epicentral azimuth Θ of the detected earthquake.

Here $X_{ns}(i)$, $X_{ew}(i)$ and $X_{ud}(i)$ are amplitudes of NS, EW and UD, α is smoothing parameter; $0 \leq \alpha \leq 1$, i shows

Table 1 Relationship between the Signs of R_{nsud} and R_{ewud} and the Quadrant of Θ

Case No.	Sign of R_{nsud}	Sign of R_{ewud}	Quadrant of Θ	Reference
1	−	−	I	N
2	+	−	II	II I
3	+	+	III	III IV
4	−	+	IV	S

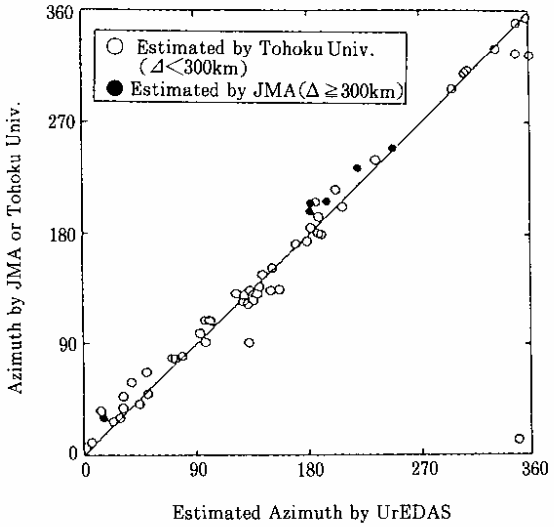

Fig. 5 Comparison of azimuth estimated by UrEDAS at Miyako and that determined by the local network of Tohoku University or the national network of JMA

time step. Table 1. gives the relationship between the signs of $R_{nsud}(i)$ and $R_{ewud}(i)$ and the quadrant of $\Theta(i)$.

Fig. 5 compares the epicentral azimuth estimated by the local network of Tohoku University or the national network of the Japan Meteorological Agency (JMA) and that by the proposed method using the data of a single UrEDAS observation point. They coincide within ±20 degrees.

(2) Magnitude of Earthquake

The magnitude of an earthquake relates to the size of a seismic fault: the larger the fault, the greater the magnitude. Also the duration and the predominant period of the shaking is proportional to the earthquake magnitude. Therefore, the magnitude of an earthquake can be predicted from the predominant period of the initial motion. The predominant period of the initial motion can be estimated by the zero-crossing method. Here, a new quick method of estimating predominant frequency, which is inverse of period, for each time step in real time is proposed (Nakamura, 1985).

An example using observed velocity v and its time differential dv/dt (= a) is shown as follows. From the analogy in the case of harmonic motion, the predominant frequency F can be defined as Eq.(4).

$$F(i) = (A(i)/V(i))^{0.5}/(2\pi) , \quad (4)$$
$$A(i) = \alpha\, A(i-1) + a(i)^2 , \quad (5)$$
$$V(i) = \alpha\, V(i-1) + v(i)^2 , \quad (6)$$

where $a(i)$ and $v(i)$ are amplitudes of acceleration and velocity at present time step i. α is smoothing parameter which is the same one in the previous section. Smoothed square amplitudes of acceleration and velocity are calculated by $A(i)(1-\alpha)$ and $V(i)(1-\alpha)$ respectively. Therefore these values are explained as follows:

$$A(i)(1-\alpha) = \int A(\omega)d\omega \quad (7)$$
$$= \int (\omega V(\omega)d\omega, \quad (8)$$
$$V(i)(1-\alpha) = \int (V(\omega)d\omega , \quad (9)$$

where $A(\omega)$ and $V(\omega)$ are power spectrums of acceleration and velocity. Then $F(i)$ is defined as a gravity center of a figure enclosed by power spectrum of velocity and frequency axis as follows:

$$F(i) = (\int \omega V(\omega)d\omega / \int V(\omega)d\omega)^{0.5}/(2\pi) \quad (10)$$

There may be considerable variation. The method proposed here is a typical one. Using this method, the predominant frequency can be estimated continuously in real-time as shown in Fig. 6. In Fig. 7 a comparison between the initial motion periods automatically read by the UrEDAS and the magnitudes given by JMA is given. The fluctuation of the magnitude estimated by UrEDAS are almost within 0.5 relative to the magnitude estimated by JMA.

(3) Hypocentral Distance

In general, the magnitude of an earthquake is predicted from the amplitude of the initial motion and the distance from the hypocenter. As the amplitude of an initial motion can be automatically measured and the magnitude of the earthquake can be estimated from the period of the initial motion, the hypocentral distance can be estimated from this information about initial motions. Although the accuracy of estimating the hypocentral distance in this way (a half to twice) is not high, more accurate estimation of the hypocentral distance by using the duration of preliminary tremors is possible after the arrival of the principal motion.

(4) Identification of P-wave and S-wave

The processing of the above mentioned information is based on the premise that the detected seismic motion is a P- wave, and identification of whether it is a P-wave or a S-wave is possible by utilizing the characteristics of the seismic wave motion incident from below, at approximately right angles to the ground surface. Namely, in principle, if the ratio V/H is greater than one (tentative value: vertical motion is predominant), it can be considered as the P-wave, and if the ratio V/H is less than one (tentative

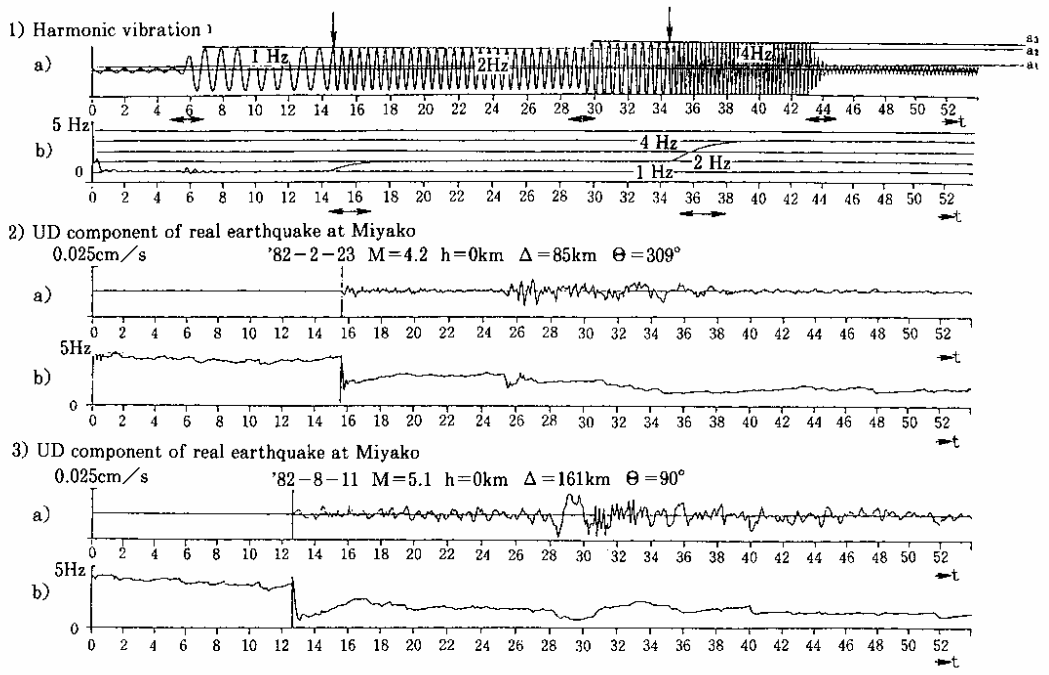

1) Harmonic ground motions and corresponding frequencies estimated automatically.

a) Harmonic ground motions of frequency 1 Hz with amplitudes a_1 and a_2, 2Hz with a_2 and a_3, and 4Hz with a_3 and a_1, where $a_1=0.0050$, $a_2=0.0250$ and $a_3=0.0300$ (unit cm/s). At times $t\fallingdotseq 5-7$ sec, 29−30 sec and 43−45sec amplitudes change from a_1 to a_2, a_2 to a_3 and a_3 to a_1 without changing frequencies (indicated as ⟷), while at times t=14.5 sec and 34.5 sec frequencies change from 1 Hz to 2 Hz and 2 Hz to 4 Hz without changing amplitude (indicated as ↓).

b) Frequency disturbance due to amplitude increase is seen clearly at $t\fallingdotseq 5-7$ sec and slightly at $t\fallingdotseq 29-31$ sec but no disturbance is seen at t=43−45 sec where amplitudes decrease. Transient shifts of predominant frequencies at t=14−17 sec and t=35−38 sec from 1 Hz to 2Hz and from 2 Hz to 4 Hz continue for about 3 sec (indicated as ⟷).

2) and 3) Actual seismic motions (a) and corresponding predominant frequencies estimated automatically (b). Predominant frequency of the ground noise before P onset is around 5 Hz and for P waves it decreases to 1−2 Hz, recovers to 2−3 Hz after 3−4 sec and again decreases slightly when S waves arrive which recover after 1−2 sec.

Fig. 6 Results of estimation for predominant frequency in real time.

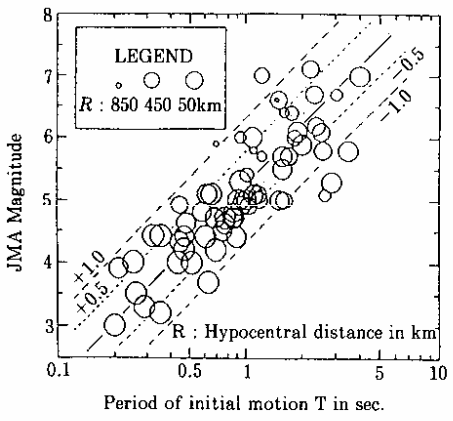

Fig. 7 Relationship between periods of initial motion automatically read by UrEDAS and the magnitudes given by JMA.

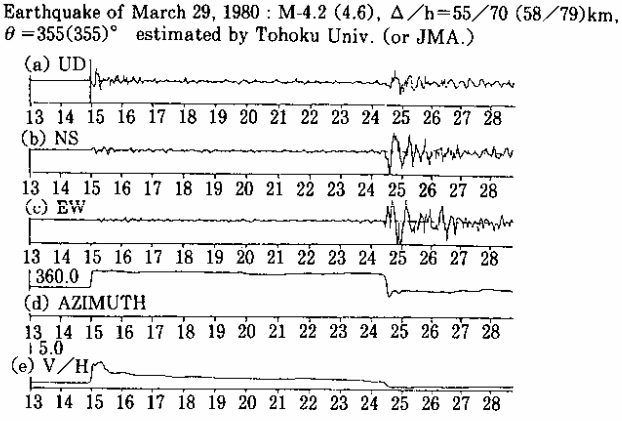

Fig. 8 Seismic wave motions recorded at Miyako(a~c), with epicentral azimuth (d) and V/H (e) estimated by UrEDAS at Miyako

value: horizontal motion is predominant), it can be considered as the S-wave (see Fig. 8). V and H are vertical and horizontal amplitude smoothed by Eqs. (11) and (12).

$$V(i)^2 = \alpha V(i-1)^2 + X_{ud}(i)^2 \quad (11)$$

$$H(i)^2 = \alpha H(i-1)^2 + X_{ns}(i)^2 + X_{ew}(i)^2 \quad (12)$$

(5) Estimation of Epicentral Distance and Depth

The epicentral distance Δ and depth h can be estimated, based on the hypocentral distance R by using as a parameter the ratio of the vertical initial motion to the horizontal initial motion. Figs. 9 and 10 Δ show the relations of V/H to Δ/R, and to h/R respectively. By means of Figs. 9 and 10, Δ and h can be estimated from V/H and R.

3.2 Examples of Earthquake Monitoring by UrEDAS

Here we present how UrEDAS functioned in times of the Northridge Earthquake, 17 January 1994, and the Hyogo-Ken-Nanbu Earthquake, 17 January 1995.

During the first 24 hours after the Northridge Earthquake, UrEDAS detected about 700 aftershocks of which their magnitudes and hypocenters were automatically determined as shown in Fig. 11. All earthquakes detected by the Pasadena UrEDAS were indicated graphically in the office room of Seismological Laboratory of Caltech immediately after each event. In addition, Pasadena UrEDAS information has been sent to CUBE and referred as useful data..

Fig. 12 shows the monitor result by UrEDAS at Kongo-San nearest to the Shinkansen line for the Hyogo-Ken-Nanbu Earthquake sequence before 30 Jan. 1995. Although it used data at a single station, aftershock activity was almost correctly traced. The Hyogo-Ken-Nanbu Earthquake occurred just beneath the San'yo Shinkansen line and alarm seismometers along the line have responded to the event. The recorded seismograms showed that strong seismic mo-

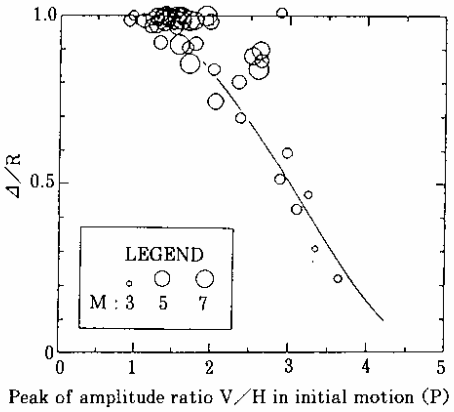

Fig. 9 Relation between V/H and Δ/R.

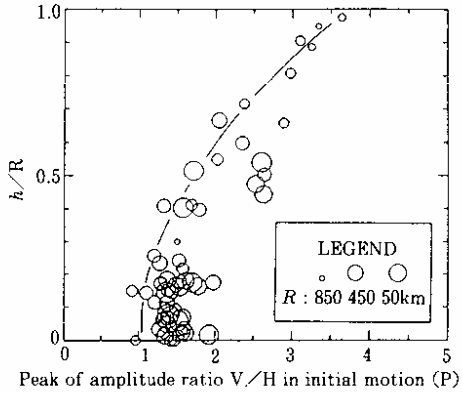

Fig. 10 Relation between V/H and H/R.

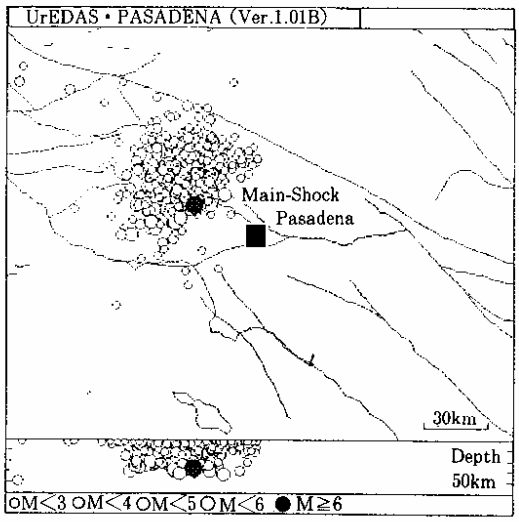

Fig. 11 The Northridge Earthquake Sequence by Pasadena UrEDAS.

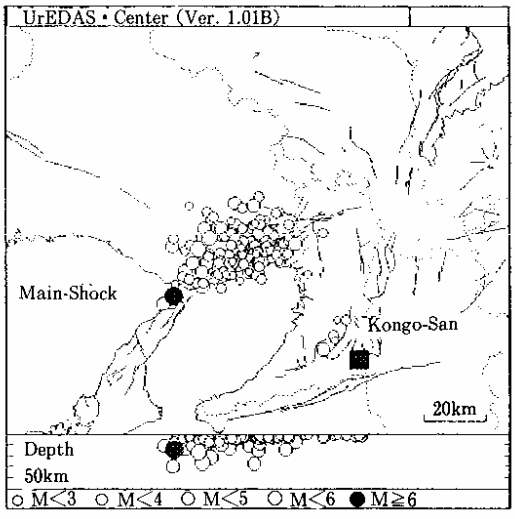

Fig. 12 The Hyogo-Ken-Nanbu Earthquake Sequence by Kongo-San UrEDAS.

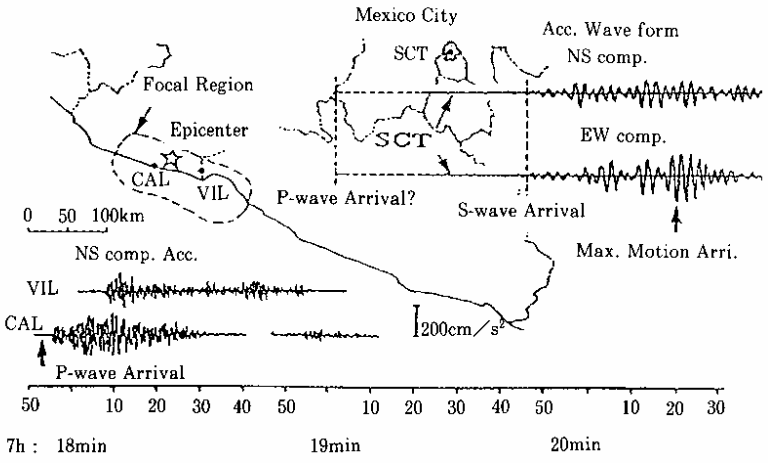

UrEDAS at CAL or VIL can issue alarm around 5 sec before or10 sec after7h 18 min for Mexico City, where maximum motion arrives after 7 h 20 min which gives about 2 minutes margin time. Even UrEDAS at Mexico City Which issues alarm by P arriving just after 7 h 19 min can give 1 minute margin time before the maximum motions.

Fig. 13 Strong motion propagation of the 1985 Michoacan Earthquake.

tions arrived successively at the alarm seismometers installed every 20 km along the line and each seismometer issued alarm within a few seconds one by one. All Tokaido UrEDAS, except the one at Gozaisho, judged the Hyogo-Ken-Nanbu Earthquake as harmless for the Tokaido Shinkansen which terminates at Shin-Osaka and did not issue the alarm. But, even granted that a P-wave alarm was issued from the Kongo-San UrEDAS, this alarm and alarms from the seismometers along the line would probably reach almost simultaneously. It suggests that the alarm seismometers along the Shinkansen line functioned as expected.

3.3 Time Margin and its Effect for Disaster Prevention

Fig. 13 shows that, if UrEDAS had been installed along the Pacific coast of Mexico and issued alarm, the P-wave of the 1985 Michoacan Earthquake would reach Mexico City one minute after the alarm and the main strong motions which caused damage reach there another one minute later. Namely there is two minutes margin time for Mexico City, and even if UrEDAS had been installed only in Mexico City, still there were one minute margin. This margin time expected by the UrEDAS in Mexico City is nearly equal to that of the Mexico City Seismic Alert System consisting of seismometers along the Pacific coast of Mexico. People can move 100 m or over per one minute. UrEDAS can decrease human damage, by utilizing this one minute margin time. Adequate refuge reaction, use of anti-shelter in high rise building floor, etc. can be recommended for use during the margin time between the alarm and strong seismic motions.

UrEDAS gives a prompt first alarm within a few seconds and provides more exact information about one minute after it detects the event. It is not only useful for the safeguard of train and automobile transportation, but also expected to be applied widely for the different disaster prevention problems as follow: trigger of active control devices of building, control of elevator of high-rise building, earthquake countermeasures of chemical plant and nuclear power plant, tsunami warning for the harbor and coastal publics, early response of fire-fighting, preparedness of hospitals, etc.

4. DURABILITY OF GROUND AND STRUCTURES (ESTIMATION OF DAMAGE)

Besides monitoring of earthquake forces, another basis for the earthquake disaster prevention is to know exactly the durability of ground and structures. It is important to grasp present durability correctly. Earthquake damage depends upon strength, period and duration of seismic motions. Besides nature of earthquake itself, these parameters reflect strongly seismic response of surface ground and structures. Thus the vulnerable weak points can be easily disclosed by examining seismic motion characteristics of surface ground and structures.

4.1 Estimation of Seismic Characteristics of Surface Ground and Structures

Characteristics of seismic motions of surface ground effective to earthquake damage can be approximately evaluated by boring investigation. However, the investigation needs much time and cost which hinders executing it at many places.

Noting the relation between horizontal and vertical earthquake motions obtained by strong motion seismometer (Nakamura and Saito, 1983a), seismic characteristics of surface ground will be approximated with the spectral ratio of horizontal to vertical components of ground surface microtremors (Nakamura, 1989). Here we name this

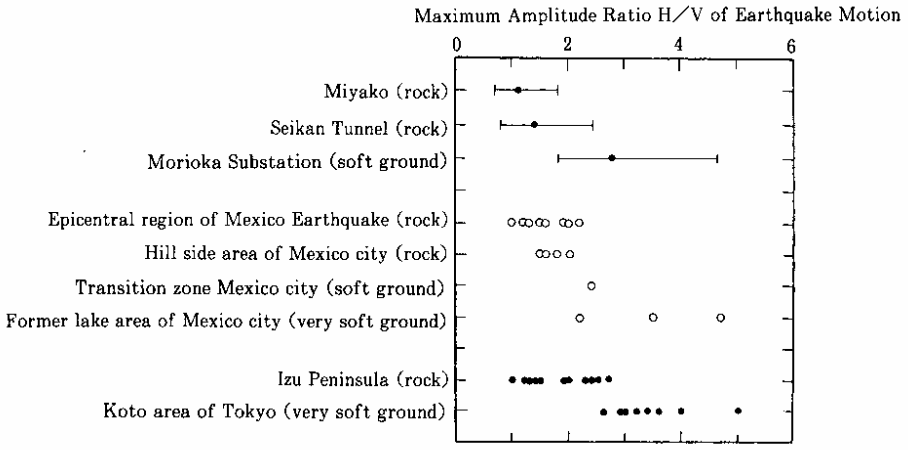

Fig. 14 Ratio of horizontal and vertical maximum acceleration (H/V) for the different surface ground conditions.

spectral ratio as QTS (Quasi-Transfer Spectrum). Natural frequency F and amplification factor A of surface ground can be correctly measured from QTS of microtremors of surface ground. This fact has been recognized by many researches with numerical experiments or field observations (for example, Lermo and Chavez-Garcia., 1993).

Seismic response characteristics of structures can be estimated from spectral ratio of microtremors observed simultaneously on the structures and on the ground surface near the structures. QTS of microtremors on the structure represents the combined characteristics of surface ground and the structure.

4.2 On the Quasi-Transfer Spectra, QTS

As shown in Fig. 14, maximum accelerations of horizontal and vertical directions are almost equal on the hard rock ground but on the soft ground the horizontal acceleration is appreciably larger than the vertical acceleration. Besides, ratio of maximum horizontal acceleration to maximum vertical acceleration has good correlation with the ratio of maximum horizontal acceleration of surface ground to maximum horizontal acceleration of basement layer as shown in Fig. 15.

Microtremors is a mixture of natural ground oscillations due to wind, rainfall, sea waves, volcanic activity and earthquakes and artificial ground vibrations due to different human activities, such as transportation (road, railway), factories, constructions, etc. Thus their origins in general cannot be identified. Especially on the hard ground which has no directional nature, there is no reason that the microtremor predominates in particular direction and the ground statistically vibrates uniformly in all directions.

Fig. 16 shows the typical geological structure of sedimentary basin. Ground motions or their spectra at different places are defined as follows:

Hr, Vr :Seismic horizontal and vertical motion on the exposed rock ground near the basin.

Hb, Vb :Seismic horizontal and vertical motion in the basement under the basin.

Hf, Vf :Horizontal and vertical spectra on the surface ground of the sedimentary basin.

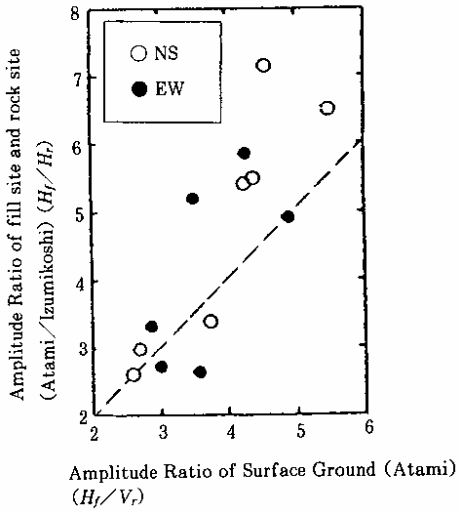

Fig. 15 Relation between ratio of maximum horizontal acceleration of sedimentary basin surface ground Hf against maximum horizontal acceleration of exposed rock ground near the basin Hr (H_f/H_r) and ratio of horizontal and vertical maximum acceleration of sedimentary basin surface ground (Hf/Hr) and ratio of horizontal and vertical maximum acceleration of sedimentary basin surface ground (H_f/H_r).

Hs, Vs :Spectra of horizontal and vertical directions of surface wave.

Ah, Av :Amplification factor of horizontal and vertical motions of vertically incident seismic body wave.

Th, Tv :Horizontal and vertical direction seismic amplification factor of surface ground of the sedimentary basin based on the seismic motion in the basement beneath the basin.

Thr, Tvr:Horizontal and vertical direction amplification factor of surface ground of the sedimentary basin based on the seismic motion on the exposed rock

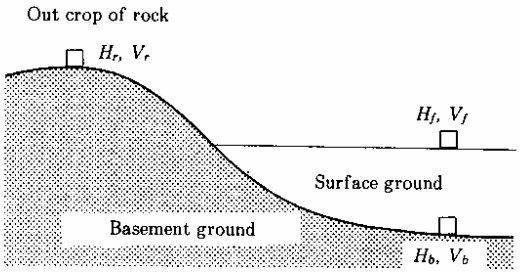

H_f, H_b, H_r : Horizontal Motion or Spectrum

V_f, V_b, V_r : Vertical Motion or Spectrum

Fig. 16 Typical structure of sedimentary basin.

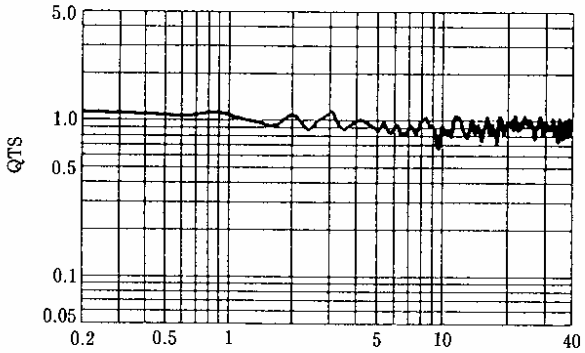

Fig. 17 QTS of microtremors of a rock site UrEDAS station, Kongo-San (cf. Fig. 12)

ground near the basin.

vb, vf :S-wave velocity in the basement beneath the basin and in the sedimentary layer.

Fig. 17 shows QTS of microtremors on the rock ground. On the solid ground, horizontal spectra and vertical spectra are almost equal within a very large frequency range.(Hr ≅ Vr, Hb ≅ Vb)

The microtremors in addition receive influence of surface waves which are originated by the amplification of surface ground and due to geometry of the border around the sedimentary basin. Thus,

$$Hf = Ah \times Hb + Hs, \quad (13)$$
$$Vf = Av \times Vb + Vs, \quad (14)$$
$$Th = Hf/Hb = Ah + Hs/Hb, \quad (15)$$
$$Tv = Vf/Vb = Av + Vs/Vb. \quad (16)$$

Generally Poisson ratio of the sedimentary layer exceeds 0.45. Thus P-wave velocity is more than three times of S-wave velocity. In very soft ground S-wave velocity is smaller than 100m/s while P-wave velocity exceeds 1000m/s due to water contents. Thus in such sedimentary layer vertical component cannot be amplified (Av ≅ 1) around the frequency range where horizontal component receives large amplification. Accordingly, if there is no effect of surface waves, Vf ≅ Vb. On the contrary, if Vf is larger than Vb, it is considered as the effect of surface waves. Then, estimating the effect of surface waves by Vf ≅ Vb (=Tv), horizontal amplification will be corrected as follows:

$$Th^* = Th/Tv = (Hf/Vf)/(Hb/Vb) = QTS/(Hb/Vb), \quad (17)$$

where QTS = Hf/Vf.

$$Th^* = QTS/(Hb/Vb) = (Ah \times Hb + Hs)/(Av \times Vb + Vs)/(Hb/Vb)$$
$$= Ah/(Av + (Vs/Vb)) + (Hs/Vs)/(Hb/Vb)/(1 + Av/(Vs/Vb))$$

As Hb/Vb ≅ 1,

$$Th^* \cong QTS \cong Ah/(Av + \beta) + (Hs/Vs)/(1 + Av/\beta), \quad (18)$$

where β = Vs/Vb which indicates the degree of influence of Rayleigh wave. When there is no influence of Rayleigh wave, namely β = 0, QTS = Ah/Av. When the influence of Rayleigh wave is large, QTS = Hs/Vs.

In the range of lowest proper frequency F of horizontal motion, Av = 1, and Hs/Vs shows a peak as well as Ah. Thus QTS shows stable peak at frequency F.(cf. Fig. 18 after Nakamura et al 1994 b) Even when influence of Rayleigh wave is large, Vs becomes small (which results in a peak of Hs/Vs) around first order proper frequency F due to multiple reflection of horizontal motions. And QTS = Ah, if microtremors of the basement Vb is sufficiently large.

Thus QTS represents the first order proper frequency due to multi-reflection of SH-wave in the surface ground layer and resulted amplification factor, regardless of the influence degree of Rayleigh waves.

In addition, if influence of Rayleigh waves becomes larger, QTS < 1 in the relatively wide range of frequency and if influence of Rayleigh waves is smaller, we can expect QTS < 1 locally, in the narrow frequency range at three times higher than F due to influence of vertical motions.

If Rayleigh waves are considered as main component of microtremors, phase difference spectraof microtremor QTS becomes ±90° in the main frequency range with high coherences. As shown in Fig. 19, although in general observation points phase spectra of QTS is random with low coherences, for very soft reclaimed land such as Marina District of San Francisco, it is clear the Rayleigh waves predominate in microtremors from the phase difference spectra with high coherence in the wide frequency range. But in the peak of QTS, the phase difference differ from ±90° and the coherence is very low. This suggests, the peak of QTS doesnt consist of Rayleigh wave.

Main waves consisting of microtremors are on one occasion either body waves or Rayleigh waves and on another occasion mixture of both waves. It depends on the locations, meteorological conditions and vibration source

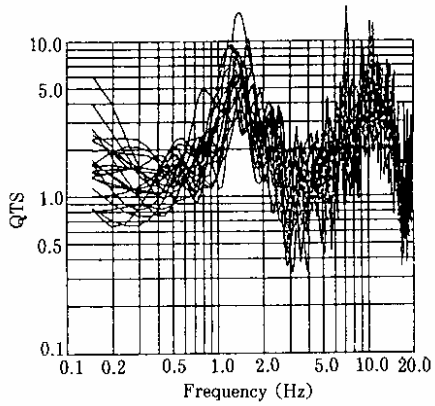

(a) QTS of NS components of microtremors observed every one hour for 24 hours at Kamonomiya, which show short period stability of QTS.

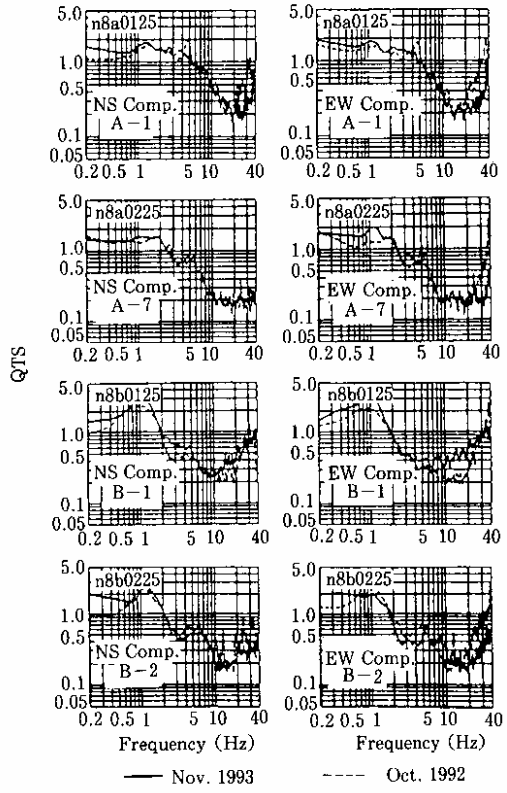

(b) QTS of NS and EW components of microtremors observed on Oct. 1992 and Nov. 1993 at sites A−1, A−7, B−1 and B−2 in Noshiro City, which show long period stability of QTS.

Fig. 18 Stability of QTS.

situations. For such microtremors, if we calculate QTS, we can estimate first order proper frequency by multiple reflections of SH-wave in the surface layer and its amplification factor correctly.

If we take the nearest exposed rock ground as a base,

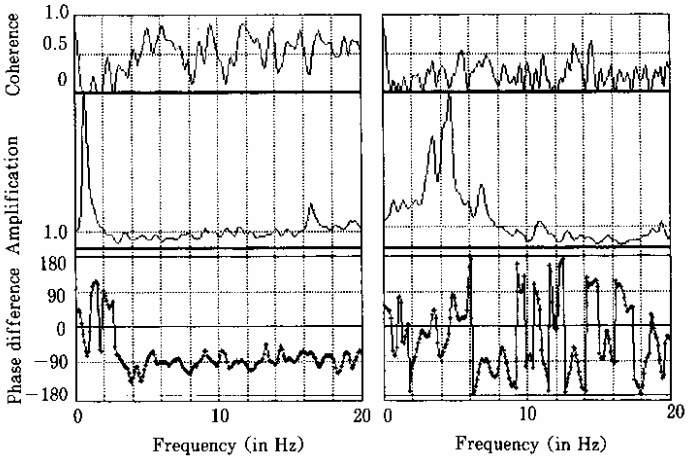

Fig. 19 Example of QTS (=Spectral ratio H/V) in Marina District, San Francisco

characteristics of surface ground Thr is given as

$$Thr = Ah + Hs/Hr \tag{19}$$

and Thr is generally larger than Ah. On the contrary , QTS of surface ground microtremors is usually smaller than Ah. Thus estimated amplification factor by Thr is larger than that by QTS.

Besides, Thr includes apparent amplified peak influenced by Rayleigh waves and there is a possibility to miss proper frequency peak of surface ground. In order to avoid this, it is necessary to omit the influence of surface waves. Applying the above mentioned procedure for the correction, QTS of surface ground microtremors is obtained.

Comparing the predominant frequency F and amplification factor A estimated from QTS of surface ground microtremors with the results of boring tests, depth of surface ground obtained by QTS reveals a correspondence to the boundary between alluvium and diluvium with high velocity contrast, and S-wave velocity of basement is estimated as nearly 600m/s.

Fig. 20 shows results of microtremor observations executed every 100m along certain railway line. HERAS, Hazards Estimation and Restoration Aid System, which will be described later, includes these results as data base. QTS of the structure and surface ground may be calculated by microtremors. Fig. 20 shows clearly that the form of QTS of surface ground corresponds very well to the geologic and topographic structures.

Until now microtremors have been measured at more than 20,000 sites mainly along the railroads every 100 m. In order to make possible such large number of microtremor measurement, PIC, Portable Intelligent Collector, was developed in 1986. Since 1986, three types of PIC, PIC86, PIC87 and PIC91, have been developed. Table 2 and Fig. 21 show the basic functions and the photographs of these PIC, respectively.

4.3 Vulnerability Indexes K-values fir Surface of Ground and Structures

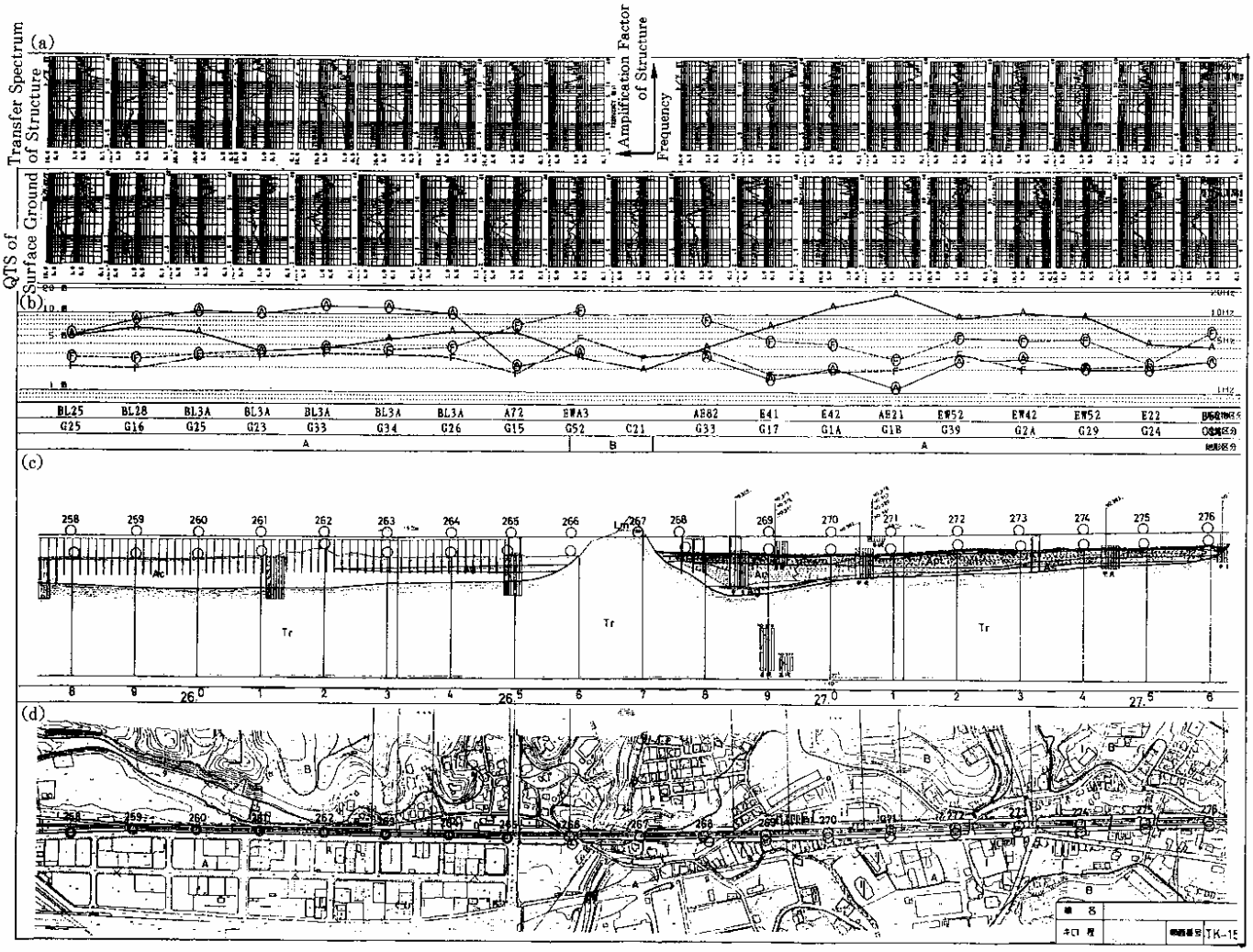

(a) Spectra of microtremors observed at sites every 100 m along the railway

(b) Distributions of predominant frequencies and its amplification factors of surface ground and structures, along the surveyed railway line.

(c) Vertical cross-section of the ground along the railway with the observation sites of microtremors, No. 258－No. 276.

(d) Topographical and geological map along the railway with the observation sites of microtremors, No.258－No.276.

Fig. 20 Basic Administration Diagram of Earthquake Disaster Prevention for Railways

Table 2 Main function of PICs

	PIC86	PIC87	PIC91
Dimensions (mm)	550W × 350D × 200H	560W × 330D × 195H	465W × 365D × 170H
Weight of Main Body	about 14 kg	about 14 kg	about 11 kg
Resolution Bit of A／D	12 bit	12 bit	16 bit with AGC
Sampling Interval (sec)	N／60	N／100	N／100, N: positive integer
Max. Recordable No. of Data	4096 Data／CH	8192 Data／CH	8192 Data／CH
Recording Media	3.5 FD (750 KB)	3.5 FD(1.2 MB)	3.5 FD(1.2 MB)
Capacity of FD	29 Files for 4096×3CH	24 Files for 4096×6CH	12 Files for 4096×6CH
CPU	Intel 8086 (5 MHz)	μPD 70216 (8 MHz)	Intel 486SX (33 MHz)
Display	3 Waveforms on 640×200LED	Max. 6 Waveforms on 640×400LED	Max. 6 Waveforms on 640×400LED
Gain	10 ～ 106 dB, 4dB step	0 ～ 120dB, 5dB step with Auto. Gain Recognition	0 ～ 60 dB, 20dB step with Auto. Gain Setting
Duration with Internal Battery	about 1 hour	about 8 hours	about 8 hours

PIC 86

PIC 87

PIC 91

Fig. 21 Different types of PIC and its sensors.

Table 3 Strain Dependence of Dynamic Properties of Subsoil Size of Strain

Size of Strain γ	10^{-6}	10^{-5}	10^{-4}	10^{-3}	10^{-2}	10^{-1}
Phenomena	Wave, Vibration		Crack, Diff. Settlement		Landslide, Soil Compaction, Liquefaction	
Dynamic Properties	Elasticity		Elasto-Plasticity		Repeat-Effect, Speed-Effect of Loading	

K-values have been proposed, in order to estimate the earthquake damage of surface ground and structures accurately.

(1) K-value of Surface Ground

For the vulnerability index K of surface ground, shear strain γ is considered. Table 3 shows the relationship between damage of foundation and size of γ (Ishihara, 1982). According to this table, ground soil becomes a plastic state at about $\gamma = 1000 \times 10^{-6}$ and for $\gamma > 10000 \times 10^{-6}$ landslide or collapse of foundation occurs.

Simplifying the shear deformation of surface ground as shown in Fig. 22, average shear strain γ can be estimated as $\gamma = Ad/H$, where A is amplification factor of surface layer, H is thickness of surface layer and d is seismic displacement of the basement. Putting the S-wave velocities of the basement and surface layer are v_b and v_f respectively, natural frequency F of the surface layer can be expressed as $F = v_b/(4HA)$. Acceleration a in the basement can be expressed as $a = (2\pi F)^2 d$, and shear strain γ is expressed as follows:

$$\begin{aligned} \gamma &= (Aa/(2\pi F)^2)(4AF/v_b) \\ &= (A^2/F)(a/\pi^2 v_b) \\ &= CKa, \end{aligned} \tag{20}$$

where, $C = 1/(\pi^2 v_b)$, (21)

$K = A^2/F$. (22)

C is expected to be almost constant for various sites. K-value is an unique value corresponding to the site and can be considered as a vulnerability index of the site, which is expected useful to select weak points of ground. Putting v_b = 600m/s (Nakamura and Takizawa., 1990), C becomes C

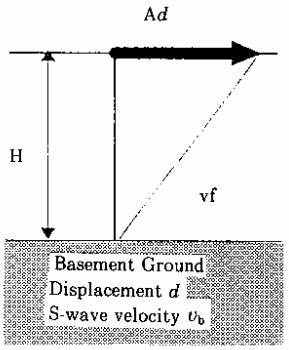

Fig. 22 Deformation of Surface Layer.

$= 1.69 \times 10^{-6}$ (s/cm). If effective strain is considered about 60% of estimated maximum strain, effective strain can be estimated by K-value multiplied with maximum basement acceleration in Gal.

Fig. 23 indicates K-values at San Francisco Marina District obtained by microtremor measurements in San Francisco Bay Area after the 1989 Loma Prieta Earthquake. According to this, the sites K>20 liquefied, while K-values in the area with no damage were much smaller. Considering the maximum accelerations near the sites, surface ground liquefied in $\gamma > 1000 \times 10^{-6}$.

(2) K-value of Column of Rigid Frame Viaduct

Concrete columns are designed in general to be collapsed by bending moment. Vulnerability index Ksg for a column of rigid frame viaduct is derived from marginal strain due to the bending moment at upper and lower ends of column. Namely, marginal strain of the upper and lower column ends are obtained by multiplying Ksg with maximum acceleration of basement layer. Ksg value for i-th story column of the two-storied rigid frame viaduct is

defined as follows (Nakamura et al., 1994, Sato et al., 1995).

$$Ksg = (7500/\pi^2)(Asg/F^2)\times(b\ h_i)/(h_1^3 + h_2^3) \quad (23)$$

where Asg is a combined amplification factor of surface ground and the viaduct itself, F (in Hz) is first order natural frequency of the viaduct, b (in m) is width of the column in vibrating direction and h*i* (in m) is column height of *i*-th story. In addition, $7500/\pi^2$ is a coefficient to adjust the calculated result to be in unit 10^{-6} strain, when seismic acceleration is measured in unit Gal (cm/s^2). The formula indicates larger Ksg for the higher column of two-storied rigid frame viaduct which receives more damage. This corresponds to the actual viaduct damage in the Hyogo-Ken-Nanbu Earthquake.

Fig. 24 shows damage of Hyogo-Ken-Nanbu Earthquake, with Ksg values calculated from the microtremor data of surface grounds and rigid frame viaducts along the Shinkansen measured at every 100m intervals before the Earthquake. The result indicates that the collapsed viaducts are found where (1) Ksg>50 and (2) Ksg values show peaks. Ksg measured before the Earthquake corresponds very well to the damage actually caused by the Earthquake. Thus, we can conclude that earthquake damage will be predicted correctly by using Ksg values obtained before the earthquake occurs.

4.4 Estimation of Maximum Acceleration

Maximum acceleration a of basement is estimated by the Nakamura-Tomita formula (Nakamura and Tomita, 1984) and acceleration of ground surface can be obtained by multiplying the amplification factor of surface ground with basement acceleration.

$$\log a = 0.168M - 0.5\log(\Delta + h) - 0.0551\times10^{-0.156M}\times\Delta + 1.86, \quad (24)$$

where M, Δ and h are magnitude, epicentral distance (km) and focal depth (km) respectively.

Fig. 25 shows maximum accelerations of surface ground along the San'yo and Tokaido Shinkansens estimated for the Hyogo-Ken-Nanbu Earthquake, Jan. 17, 1995, using the above method. Maximum accelerations along the line recorded at the train stations and transformer stations are approximately equal to the estimated values.

5. ESTABLISHMENT OF HERAS

HERAS, Hazards Estimation and Restoration Aid System, is a system which estimates a detailed earthquake damage situation promptly by receiving information from UrEDAS, and using investigation results of vibration characteristics of foundation grounds and structures obtained by microtremors (results of microzonation) as data base (see Fig. 26). By estimating the impending damage situation in detail, HERAS helps rapid and reasonable restoration of railway operation. HERAS is able to show the estimated results in visual form pictures and in numerical tables within a few minutes after the earthquake. HERAS also can help reasonable routine maintenance and use its function in ordinary time.

As explained in the previous sections, vulnerability indexes K-values, defined for surface grounds, embankment , and structures such as rigid frame viaduct, are useful to estimate earthquake damage correctly. At present HERAS predicts and illustrates the damage by statistical methods within 5 minutes. A new HERAS which can give much more precise damage prediction using K-values, is being developed as a heart of the general disaster prevention system, which can be used for complex disaster combined with various natural disasters such as flood and earthquake.

6. CONCLUDING REMARKS

Natural disasters isolate every one from others and autonomous judgment and action of individual person becomes important. Disaster prevention system itself may be

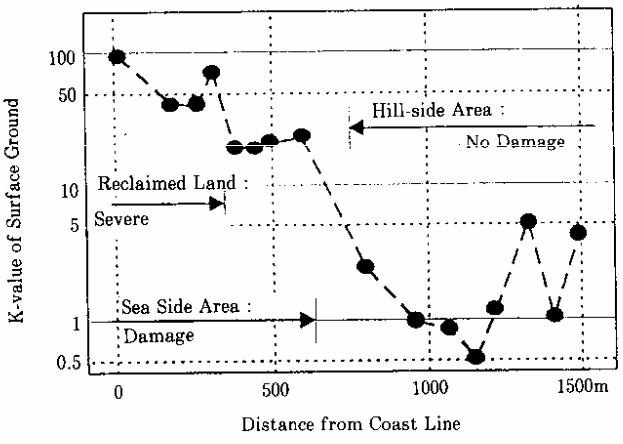

Fig. 23 K-values in S.F. Marina District.

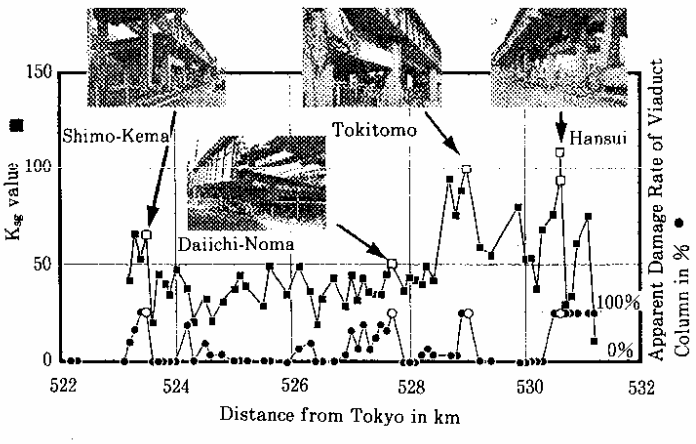

Fig. 24 Comparison of the damage and K_{sg} values of rigid frame viaducts of San'yo Shinkansen

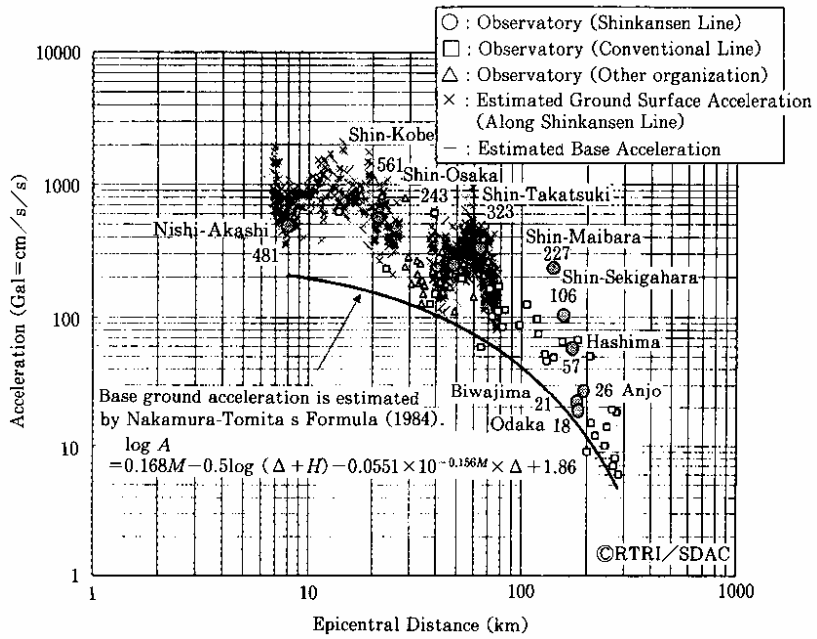

Fig. 25 Maximum Accelerations along the Shinkansen lines estimated by the formula Nakamura-Tomita (24) (×) and several observed values (○, □, △) of the 1995 Hyogo-ken-Nanbu Earthquake.

also isolated in time of disasters. Thus UrEDAS was planned as a system which can function autonomously without human interference. and does not presume network operation Of course, plural UrEDAS can work as a network to give synthetic information with higher accuracy to HERAS.

On the contrary, for HERAS communication with human work is important because HERAS is expected to help human action for the rapid, reasonable restoration works. The system may become out of order or stop receiving information. Then the operators who use the system should use information from the system carefully and utilize it autonomously, checking it with information from other sources. The author hopes in the future to develop disaster prevention systems such as UrEDAS and HERAS helping autonomous human actions for the disaster prevention.

7. ACKNOWLEDGMENT

The author is grateful to the staffs of Seismological Laboratory, California Institute of Technology with Prof. Hiroo Kanamori and of United States Geological Survey for their cooperation to test UrEDAS in Pasadena, California, USA. Thanks are due to Japan Railway Companies, who have strongly helped the development and implementation of our earthquake disaster prevention systems. Ex-Prof. Setumi Miyamura of Univ. of Tokyo (present consultant of System and Data Research Inc.) has helped the author and thanks are also due to him. The author also thanks to Dr. W. H. K. Lee, former staff of USGS, for his fruitful comments.

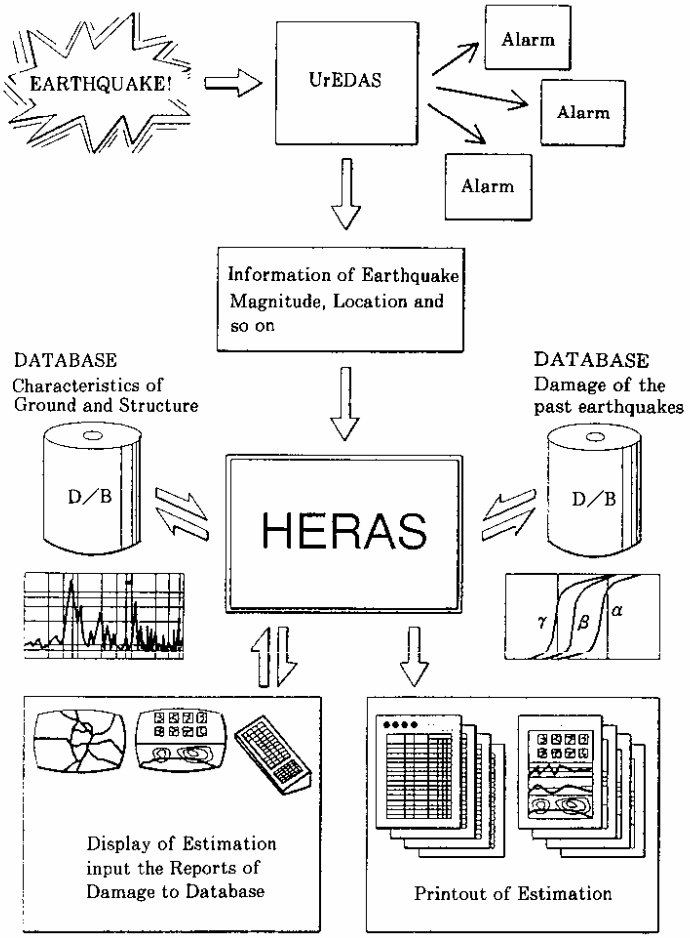

Fig. 26 Block Diagram of HERAS.

8. REFERENCE

Espinosa-Aranda, J.M., A. Jimenez, G. Ibarrol, F. Alcantar, M. Inostroza and S. Maldonaldo (1995). Mexico City Seismic Alert System. Seismological Research Letters 66(6), 42-53.

Ishihara, K. (1982). Evaluation of Soil Properties for Use in Earthquake Response Analysis. Proceedings of. International Symposium on Numerical Model in Geomechanics, 237-259.

Lermo, J. and F.J.Chavez-Garcia (1993). Site Effect Evaluation using Spectral Ratios only One Station. Bulletin of the Seismological Society of America 83, 1574-1594.

Nakamura, Y. and A. Saito (1982). Train Stopping System for Tohoku Shinkansen (in Japanese). Proceedings of Semiannual meeting of the Seismological Society of Japan 82 (2), 244.

Nakamura, Y., A. Saito and T. Hashimoto (1983). Real-Time Estimation System of Earthquakes using a Personal Computer (in Japanese). Proceedings of Semiannual meeting of the Seismological Society of Japan 82 (2), 138-139.

Nakamura, Y. and A. Saito (1983a). Amplification Characteristics Estimation of Surface Ground based on Strong Motion Records (in Japanese). Proceedings of 17th Earthquake Engineering Symposium of Japan Society of Civil Engineers, 25-28

Nakamura, Y. and A. Saito (1983b). P/S Phase Recognition of Seismic Waves and Epicentral Azimuth Using Single Station Data (in Japanese). Proceedings of 17th Earthquake Engineering Symposium of Japan Society of Civil Engineers, 95-98

Nakamura, Y. and K. Tomita (1984). Statistical Estimation Formula for Maximum Seismic Ground Acceleration (in Japanese). Proceedings of 39th Annual Meeting of Japan Society Civil Engineers (I), 785-786

Nakamura, Y. (1985). A Concept of One Point Detection System and its Example Using Personal Computer for Earthquake Warning (in Japanese). Proceedings of 18th Earthquake Engineering Symposium of Japan Society of Civil Engineers, 505-508

Nakamura, Y. and B. E. Tucker (1988). Japans Earthquake Warning System -Should it be imported to California?-. California Geology (2), 33-40

Nakamura, Y. (1988). On the Urgent Earthquake Detection and Alarm System. Proceedings of 9th WCEE (7), 673-678.

Nakamura, Y. (1989). A Method for Dynamic Characteristics Estimation of Subsurface using Microtremor on the Ground Surface. Quarterly Report of Railway Technical Research Institute 30 (1), 25-33.

Nakamura, Y. and T. Takizawa (1990). The Surface Layer Thickness and the Shearing Wave Velocity of Basement and Surface Estimated by Microtremor Measurement (in Japanese), Railway Technical Research Institute Report 4 (9), 29-35.

Nakamura, Y., K. Hidaka, S. Sato and M. Nishinaga (1994). On the Vulnerability Indexes of the Rigid Frame Viaduct and the Embankment against Earthquake Motion (in Japanese with English abstract, Railway Technical Research Institute Report 8 (5), 25-28.

Nakamura, Y., K. Tomita and M. Nishinaga (1994) On the Influence of Frozen Ground upon the characteristics of Earthquake Motions of the Surface Layer (in Japanese with English abstract), Railway Technical Research Institute Report 8 (5), 41−46

Sato, S. , Y. Nakamura and M. Nishinaga (1995). Damage Analysis of Rigid Frame Viaduct of Railway caused by the 1995 Hyogo-Ken-Nanbu Earthquake (in Japanese), Proceedings of 23rd Earthquake Engineering Symposium of Japan Society of Civil Engineers, 265-268.

Appendix: Operating Result of Alarms for the Tokaido Shinkansen

The earthquake warning system for the Tokaido Shinkansen consists of the conventional alarm seismometers which respond to the strong shocks near the line and the UrEDAS which responds to the big earthquakes far from the line. Table 4 shows alarm operation results since UrEDAS started operation in March 1992. The conventional line ordinary alarms were issued in average once or twice in a year before 1992. Since around 1993, relatively big earthquakes occurred frequently in Japan, and especially in 1995 many small shocks occurred near the Tokaido Shinkansen line. Thus, during the last few years a number of alarms issued by the line alarm seismometers increased about three times against the previous years. In 1992 when UrEDAS was first used, alarms were issued rather frequently, because the UrEDAS was operated to issue alarms for relatively small earthquakes with $M>4.5$, in order to confirm the function of UrEDAS. But the number of alarms decreased and the expected function was nearly realized after the alarm target was limited to the initially considered earthquakes with $M>5.5$.

By the way, until 1993 strong electro-magnetic noise given to the seismometer out-put due to lightning near the UrEDAS station gave false alarms twice and seismic coda waves of distant large earthquakes gave other false alarms three times. After these false alarm events, soft-wares of the UrEDAS were improved and since then no false alarm has been issued, although several times lightning near the UrEDAS station and distant big earthquakes occurred..

Among three recent alarm issues of the UrEDAS, for two cases, i.e. for the 1994 Middle Shiga Earthquake M_{JMA} 5.3 with a maximum acceleration of 84 Gal recorded by the line alarm seismometer and for the 1995 Hyogo-Ken-Nanbu Earthquake M_{JMA} 7.2 (M_W 6.8, estimated by USGS) with a maximum acceleration of 323 Gal recorded by the line alarm seismometer, the conventional line alarm seismometers also issued alarms. The remaining one case was for the Far-off Tokaido Earthquake M_{JMA} 6.2, which had a focal depth of about 400 km and the conventional line seismometers did not react. As we have succeeded to discriminate deep earthquakes from near earthquakes, UrEDAS will be improved in the near future not to issue alarms for such harmless deep earthquakes. Although till now the line alarm seismometer recorded accelerations over 80 Gal eight times, including the Hyogo-Ken-Nanbu Earthquake which gave destructive damage, seven events except the latter resulted in no damage. For the seven earthquakes except the Hogo-Ken-Nanbu Earthquake, UrEDAS proposed to start

Table 4 Operation Results of UrEDAS and Ordinary Alarms for the Tokaido Shinkansen Between Mar. 92 and Mar.96

Period	Number of Issuing the UrEDAS Alarm		Number of Issuing the Ordinary Alarm		Total Number
	Total No.	M-Δ:M>4.5 in 92,M >5.5 in other yr.	PGA>40Gal with 5Hz LPF	Total No.	
Mar.－Dec. 92	10	◎ ● ● ○ ○ ○ ○ ○ ○ ○	□	1	11
Jan.－Dec. 93	4	◎ ◎ ○○	□□□	3	7
Jan.－Dec. 94	1	◙	□□□	4	4
Jan.－Dec. 95	2	○ ◙	□□□□□	6	7
Jan.－Mar. 96	0		□	2	2

○UrEDAS Alarm M>4.5　　Ordinary Alarm
◙UrEDAS Alarm M>5.5　　Ordinary Alarm and UrEDAS Alarm M>5.5
◎ UrEDAS False Alarm caused by coda wave after the distant big earthquake
● UrEDAS False Alarm caused by the lighting electromagnetic noise

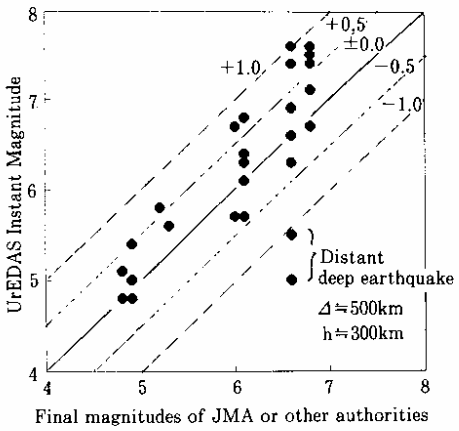

(a) UrEDAS Instant Magnitudes versus Final magnitudes of JMA or other authorities.

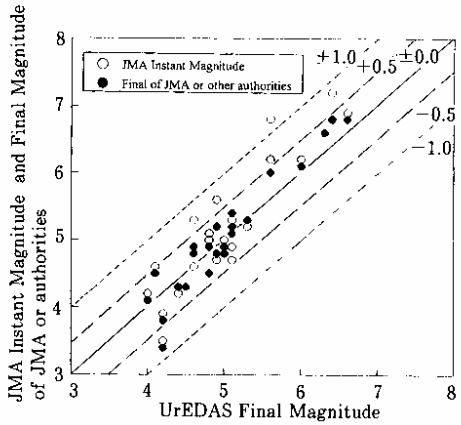

(b) JMA Instant Magnitudes and Final magnitudes of JMA or other authorities versus UrEDAS Final Magnitudes

Fig. 27 Comparison of magnitudes estimated by UrEDAS and other authorities

immediate operation to secure unconditional safety or to recover operation for a certain line section with gradual velocity increase by confirming the safety. Thus the recovery times of 2-5 hours of the train operation due to the previous reopening procedures have been reduced to 15-60 minutes. It suggests UrEDAS is useful not only for the rapid warning but also very effective for the rapid recovery after the warning.

Fig. 27 indicates the comparison between the final earthquake magnitudes of JMA and UrEDAS instant magnitude estimated within 4 seconds (a), and the comparison between unified UrEDAS final magnitudes and instant magnitudes of JMA or more accurate magnitudes estimated by other authorities (b). The figure (a) shows the UrEDAS instant magnitudes coincide with the magnitudes estimated by authorities within −0.5～+1.0 (±0.7) errors except in the distant stations for the deep earthquake. The figure (b) shows the UrEDAS final magnitudes coincide with the more accurate magnitudes estimated by authorities within ±0.5 errors. The instant magnitudes of JMA and the more accurate magnitudes estimated by authorities differ by a maximum 0.8 and UrEDAS instant magnitudes determined by a single station information can be said to have enough accuracy.